

1 **Reward integration in prefrontal-cortical and ventral-hippocampal nucleus accumbens**
2 **inputs cooperatively modulates engagement**

3
4 *Eshaan S. Iyer¹, Peter Vitaro², Serena Wu¹, Jessie Muir^{4,5}, Yiu Chung Tse², Vedrana*
5 *Cvetkovska², Rosemary C. Bagot^{2,3}*

6
7 1. Integrated Program in Neuroscience, McGill University, Montréal, Canada
8 2. Department of Psychology, McGill University, Montréal, QC, Canada
9 3. Ludmer Centre for Neuroinformatics and Mental Health, Montréal, QC, Canada
10 4. Center for Neuroscience, University of California, Davis; Davis, 95618, USA.
11 5. Department of Neurology, School of Medicine, University of California, Davis; Sacramento,
12 95817, USA.

13
14 **Abstract**

15
16 The NAc, a highly integrative brain region controlling motivated behavior, is thought to receive
17 distinct information from various glutamatergic inputs yet strong evidence of functional
18 specialization of inputs is lacking. While circuit neuroscience commonly seeks specific functions
19 for specific circuits, redundancy can be highly adaptive and is a critical motif in circuit
20 organization. Using dual-site fiber photometry in an operant reward task, we simultaneously
21 recorded from two NAc glutamatergic afferents to assess circuit specialization. We identify a
22 common neural motif that integrates reward history in medial prefrontal cortex (mPFC) and
23 ventral hippocampus (vHip) inputs to NAc. Then, by systematically degrading task complexity,
24 dissociating reward from choice and action, we identify key circuit-specificity in the behavioral
25 conditions that recruit encoding. While mPFC-NAc invariantly encodes reward, vHip-NAc
26 encoding is uniquely anchored to loss. Ultimately, using optogenetic stimulation we demonstrate
27 that both inputs co-operatively modulate task engagement. We illustrate how similar encoding,
28 with differential gating by behavioral state, supports state-sensitive tuning of reward-motivated
29 behavior.

30
31 **INTRODUCTION**

32 Redundancy is a defining property of nervous system organization (Marder, 2011; Marder &
33 Goaillard, 2006; Mizusaki & O'Donnell, 2021) yet there has been limited consideration of the
34 role of redundancy in neural circuit mechanisms of motivated behavior. Redundancy in neural
35 circuits may confer various advantages, including increasing robustness of cognition and
36 behavior to perturbation, enhancing encoding accuracy, and facilitating coherent integration of
37 multiple inputs, suggesting it should be a frequently observed motif (Ghanbari et al., 2023;
38 Hiratani & Fukai, 2018; Nguyen et al., 2019). While the literature abounds with examples of
39 apparent circuit-specific cognitive and behavioral functions, the potential for redundancy is
40 rarely examined. To better understand these opposing motifs in nucleus accumbens (NAc)
41 circuits we leveraged dual circuit recordings and computational modeling to rigorously test the
42 specificity and redundancy of information processing in a fully controlled, within animal
43 comparison of two NAc glutamatergic inputs.

45 The NAc integrates glutamatergic inputs with dopaminergic input from the ventral tegmental
46 area, with multiple glutamatergic inputs converging at the level of individual medium spiny
47 neurons in the NAc medial shell (Britt et al., 2012; Carter et al., 2007; Christoffel et al., 2021;
48 Floresco, 2015; French & Totterdell, 2002; Lind et al., 2023; Muir et al., 2024; O'Donnell &
49 Grace, 1995). Prominent theoretical perspectives hold that these inputs send qualitatively
50 distinct information which the NAc then integrates to orchestrate motivated behavior (Floresco,
51 2015; Grace et al., 2007; Lind et al., 2023; Parker et al., 2022). For example, the mPFC
52 contributes information about rewarding events and executive control while the vHip contributes
53 emotional context and behavioral inhibition (Bagot et al., 2015; Barker et al., 2019; Hamel et al.,
54 2022; Lindenbach et al., 2022; Muir et al., 2020; Otis et al., 2017; Parker et al., 2022; Spellman
55 et al., 2021; Wenzel et al., 2023; Yoshida et al., 2020). Despite predictions of distinct encoding
56 and behavioral function for mPFC-NAc and vHip-NAc, strong evidence of functional
57 specialization is lacking. To date, most studies have examined a single input and the few
58 studies that examined one or more inputs in the same task compared across animals leaving
59 open the possibility that inter-individual variation in behavior and other variables influence neural
60 encoding (Britt et al., 2012; Chen et al., 2023; Reed et al., 2018).

61
62 To systematically interrogate functional redundancy versus specialization we simultaneously
63 probed neural encoding using dual-site *in vivo* fiber photometry to record activity in two
64 glutamatergic circuits during reward-guided choice in a two-armed bandit task. The mPFC-NAc
65 is widely appreciated to mediate reward processing and, given that vHip-NAc inputs converge
66 with mPFC-NAc, we asked if the vHip-NAc might also contribute to this function (Otis et al.,
67 2017; Parker et al., 2022; Spellman et al., 2021). Using trial-by-trial modeling of neural activity,
68 we identify a novel mechanism for integrating outcome information across trials that is common
69 to both circuits. Analyzing the redundancy across signals revealed an additional dimension of
70 uniqueness to vHip-NAc encoding. By sequentially degrading task complexity we show that,
71 despite sharing a common mechanism for outcome integration, each circuit is recruited in
72 distinct behavioral states, with the vHip-NAc preferentially encoding reward after loss.
73 Optogenetically manipulating circuit-specific activity revealed that, once recruited, both inputs
74 cumulatively mediate dynamic behavioral engagement. Our findings reveal co-operative circuit
75 organization in NAc wherein redundant encoding in two inputs is gated by circuit-specific
76 mechanisms for state-sensitive tuning of reward-motivated behavior.

77

78 **Results**

79

80 *mPFC-NAc and vHip-NAc similarly encode outcomes in a probabilistically rewarded*
81 *environment*

82

83 To assess redundancy versus specificity in outcome encoding in two distinct circuits under
84 matched conditions and trial histories, we injected retrograding AAV-GCaMP7f in NAc medial
85 shell and implanted optic fibers in mPFC and vHip to record Ca^{2+} -associated fluorescence while
86 mice engaged in reward-guided choice (Fig. 1E). We trained mice in a two-lever probabilistic
87 reward learning task (i.e. a two-armed bandit task) in which lever pressing probabilistically earns
88 a chocolate milk reward (Fig. 1A). Following each lever press, one of two different auditory cues

89 signaled trial outcome (rewarded, unrewarded) and start of the inter-trial interval (ITI). To
90 maintain a dynamic environment with robustly encountered rewarded and unrewarded
91 outcomes, levers were probabilistically rewarded on 80% or 20% of presses with probabilities
92 switched after five consecutive responses on the high probability lever. Female (n=10) and male
93 (n=12) mice experienced similarly high numbers of unrewarded and rewarded trials and low
94 numbers of omission trials (Fig. 1B-D). Examining behavior across sessions shows decreasing
95 staying probability after unrewarded outcomes and increasing rewards earned, indicating
96 animals use information about outcomes to guide behavior (Fig. S1).

97

98 Trial based tasks are ideal for probing neural encoding, generating large numbers of trials.
99 However, standard analysis approaches either analyze individual trials, failing to account for the
100 within animal nested data structure and inappropriately inflating effects, or average all trials
101 within animals, thereby underestimating effects. Choice tasks are additionally challenging with
102 the number of instances of each trial type varying across animals. To preserve the power of
103 trial-by-trial data while accounting for the nested structure and unbalanced observations we
104 used a linear mixed model approach (Yu et al., 2022). To examine how outcome is encoded in
105 each projection, we modeled normalized Ca^{2+} -associated fluorescence change as a function of
106 trial outcome, while controlling for inter-individual variability.

107

108 Reward strongly suppressed mPFC-NAc and vHip-NAc activity in female and male mice. In
109 mPFC-NAc, a peak following the lever press and outcome delivery is followed by gradually
110 emerging reward-associated suppression across the ITI (Fig 1H,J,P,Q). In vHip-NAc, an initial
111 peak is followed by suppression after the lever press and outcome delivery, with suppression
112 sustained following reward or activity gradually increasing following unrewarded outcomes (Fig.
113 1 L,N,R,S). We focused analysis on the end of the ITI (8-10 sec after lever press) when trial
114 outcome has been integrated prior to next trial start. By ITI end, reward robustly suppressed
115 mPFC-NAc activity in female and male mice (Fig. 1I,K). Reward also robustly suppressed vHip-
116 NAc activity in female and male mice (Fig. 1M,O). This indicates that outcome encoding
117 emerges across the ITI with reward suppressing mPFC-NAc and vHip-NAc activity. To explore
118 modulation by other task factors, we examined neural encoding time-locked to licking and
119 decision-relevant behaviors. We did not observe clear neural encoding of licking (Fig. S2A,D),
120 the identity of the chosen lever (Fig. S2B,E), or the decision to stay or shift (Fig. S2C,F)
121 suggesting that outcome is the primary source of modulation in mPFC-NAc and vHip-NAc in this
122 task.

123

124 Having observed that mPFC-NAc and vHip-NAc are similarly modulated by reward, we then
125 examined if one circuit leads the other. Calculating the time lag for the maximum cross-
126 correlation, we found that the regression coefficients of the mPFC-NAc and vHip-NAc cross-
127 correlation did not significantly differ from zero in rewarded or unrewarded trials in either sex.
128 This shows that neither circuit drives outcome encoding in the other (Fig. S3A, B). However, we
129 observe that suppression emerges earlier in vHip-NAc than mPFC-NAc, suggesting that while
130 overall encoding might be similar, the underlying dynamics likely vary between the pathways
131 (Fig. S3C).

132

133 *mPFC-NAc and vHip-NAc similarly integrate reward history*

134

135 We find that mPFC-NAc and vHip-NAc similarly encode outcomes. Observing that reward-
136 induced suppression lasted throughout the ITI, we speculated that this enduring modulation
137 might integrate reward information across successive trials and that this integration might be
138 more prominent in mPFC-NAc than vHip-NAc, given prior evidence of enduring representation
139 in mPFC (Parker et al., 2022; Spellman et al., 2021; Sul et al., 2010). To test this, we sorted
140 trials by both prior and current outcome, identifying trial sequences that were rewarded then
141 rewarded (R→R), rewarded then unrewarded (R→U), unrewarded then rewarded (U→R), and
142 unrewarded then unrewarded (U→U). We then compared neural activity across the ITI on the
143 most recent trial to determine how prior outcome modulates outcome encoding on the current
144 trial. Analyzing males and females separately revealed similar modulation (Fig. S4) and we
145 therefore report sex-combined analyses. Both previous and current outcome modulate mPFC-
146 NAc activity (Fig. 2A). Following a given trial (t -1), reward suppresses mPFC-NAc activity (Fig.
147 2B) effectively resetting the baseline for the next trial. Reward on the subsequent trial (t0)
148 similarly suppresses mPFC-NAc by ITI end, regardless of prior outcome. However, when mice
149 are unrewarded on the subsequent trial (t0), suppression of mPFC-NAc by prior reward is
150 maintained through ITI end (Fig. 2C). This suggests that a single reward maximally and
151 enduringly suppresses mPFC-NAc activity and that, in the absence of subsequent reward, this
152 suppression slowly dissipates.

153

154 We then examined if vHip-NAc similarly integrates outcomes (Fig. 2D). Following a given trial (t-
155 1), reward suppresses vHip-NAc activity (Fig. 2E). As with mPFC-NAc, this resets the baseline
156 for the next trial (t0), wherein reward suppresses vHip-NAc regardless of prior outcome.
157 However, when the subsequent trial (t0) is unrewarded, suppression of vHip-NAc activity by
158 prior reward is maintained through ITI end (Fig. 2F). Together, this shows that mPFC-NAc and
159 vHip-NAc similarly integrate outcomes across trials. In both circuits, reward maximally
160 suppresses neural activity and activity gradually increases following subsequent unrewarded
161 outcomes, such that, by ITI end, the relative degree of suppression represents an integrated
162 reward outcome history.

163

164 *mPFC-NAc and vHip-NAc are differentially sensitive to loss*

165

166 Analyzing neural encoding of reward and outcome integration revealed that mPFC-NAc and
167 vHip-NAc similarly encode reward suggesting they may provide redundant information to the
168 NAc. To test redundancy between mPFC-NAc and vHip-NAc we calculated the conditional
169 entropy of mPFC-NAc given vHip-NAc ($\square(mPFC-NAc|vHip-NAc)$) and vHip-NAc given mPFC-
170 NAc ($\square(vHip-NAc|mPFC-NAc)$). In this way, we assessed the information contributed by each
171 circuit beyond that contributed by the other at ITI end, when outcome is fully integrated (Fig.
172 3A). We contrasted entropy between rewarded and unrewarded outcomes as a function of prior
173 outcome. Relative to unrewarded outcomes, the entropy of mPFC-NAc given vHip-NAc was
174 reduced by rewarded outcomes, indicating that vHip-NAc and mPFC-NAc signals are more
175 redundant after reward than non-reward (Fig. 3B). In contrast, following previous unreward, but
176 not previous reward, current reward increased the entropy of vHip-NAc given mPFC-NAc (Fig.

177 3C), indicating that, under these conditions, mPFC-NAc explains less of the vHip-NAc signal.
178 This shows that, after reward, vHip-NAc and mPFC-NAc encoding converges, becoming more
179 redundant, but when reward is made more surprising by immediately following loss, vHip-NAc
180 carries additional information. That is, despite global redundancy in reward encoding motifs, we
181 identify a dimension of circuit specificity and a potential unique role for vHip-NAc in encoding
182 reward following loss.

183
184 If this is true, across outcome histories, vHip-NAc encoding should be most apparent when
185 reward follows an unrewarded outcome, whereas, following consecutive rewards, vHip-NAc
186 should become insensitive to outcome as rewards become less surprising. In contrast, mPFC-
187 NAc encoding is predicted to be relatively invariant across outcome histories. To test this, we
188 examined current outcome encoding at ITI end while considering prior outcomes up to three
189 trials back. Consistent with our prediction, mPFC-NAc encoded current outcome regardless of
190 prior outcome history (Fig. 3D; Supplementary Table 1) while vHip-NAc failed to encode current
191 outcome after two or more consecutive rewards (Fig. 3E; Supplementary Table 1). This
192 supports our hypothesis that vHip-NAc encoding anchors to loss such that it is specifically
193 engaged by surprising rewards whereas mPFC-NAc invariantly encodes outcome.

194
195 *Degrading task requirements reveals circuit-specific roles in reward integration*
196
197 Analyzing informational redundancy and encoding across varying outcome histories suggested
198 that, while mPFC-NAc and vHip-NAc encode and integrate reward via a common mechanism,
199 each may nevertheless serve distinct functions in reward processing. To isolate the specific
200 conditions under which each circuit integrates outcomes we recorded neural activity while
201 degrading task requirements to sequentially eliminate choice and action. We first eliminated
202 choice, extending only a single lever while maintaining the requirement to press to elicit an
203 outcome. To hold outcome experience constant, the specific sequence of reward and unreward
204 was yoked to each animal's prior performance on the two-lever task (Fig. 4A). In the absence of
205 choice, mPFC-NAc continued to encode previous and current outcome (Fig. 4B). On trial t0, by
206 ITI end, current and prior outcomes were encoded, as in the two-lever task (Fig. 4C, Fig. 2C).
207 Examining vHip-NAc in the one-lever task also revealed largely similar outcome-mediated
208 modulation (Fig. 4D, Fig. 2D). At ITI end, prior and current outcomes were integrated, similar to
209 the two-lever task (Fig. 4E, Fig. 2F). Despite conserved information encoding in both circuits,
210 the shape of the vHip-NAc signal was more visibly altered than the mPFC-NAc. In particular, the
211 vHip-NAc signal in the one-lever task appeared noisier and blunted with the expected peak
212 following lever press largely absent, potentially suggesting heightened sensitivity to task
213 structure. Overall, we find that both mPFC-NAc and vHip-NAc maintain similar graded
214 representations of reward history that are largely independent of choice requirements.

215
216 Removing lever choice minimally impacted reward integration. We then asked if neural
217 integration of outcome history is entirely independent of response requirements by removing
218 both levers in a choice-free response-free task. Trials continued to be signaled by cue-lights, but
219 without lever extension and outcomes were passively delivered yoked to each animal's
220 individual performance on the full two-lever task (Fig. 4F). Eliminating the response requirement

221 markedly and distinctly altered reward integration in both circuits. In mPFC-NAc (Fig. 4G),
222 encoding of prior outcome was erased and only the current outcome encoded (Fig. 4H). This
223 differs from both the two-lever and one-lever tasks wherein mPFC-NAc encoded a graded
224 representation of reward history and suggests that mPFC-NAc integrates reward history only in
225 instrumental settings where a response elicits outcomes. However, even when rewards are
226 passively encountered (i.e. when no lever press is required), mPFC-NAc continues to encode
227 reward but with a shortened time constant, such that only the most recent outcome is retained.
228
229 vHip-NAc representation of reward history was also degraded, yet in a distinct manner (Fig. 4I).
230 Current outcomes were encoded only when the previous trial, t-1, was unrewarded, suggesting
231 a dependence on loss (Fig. 4J). This shift in encoding translates into vHip-NAc effectively
232 overlooking isolated instances of non-reward, likely reflecting an extended time constant.
233 Critically, this cannot be explained by changes in task engagement given that mPFC-NAc
234 continued to represent reward in these same animals (Fig. 4G,H) and licking bouts were
235 similarly maintained across task variants (Fig. S5). Rather, this reveals that task demands
236 differently shape neural encoding of reward in mPFC-NAc and vHip-NAc. When reward is
237 passively encountered, independent of a required response, mPFC-NAc maintains a simplified
238 reward representation across a shortened temporal window, limiting integration across trials. In
239 contrast, vHip-NAc anchors encoding to loss with an extended time constant, to preferentially
240 represent surprising rewards. This suggests that while the fundamental function of mPFC-NAc
241 in rewarding contexts is to encode outcomes, the fundamental function of vHip-NAc is to use
242 loss to tune outcome encoding.
243

244 *mPFC-NAc and vHip-NAc modulate task engagement*

245
246 Examining neural representation of outcomes identified both mechanistic redundancy and
247 functional specificity in mPFC-NAc and vHip-NAc encoding. We then asked how this neural
248 processing might integrate to modulate behavior. While in general encoding was similar in both
249 circuits, reducing the requirement for engagement by making reward non-contingent revealed
250 functional specialization. We hypothesized that outcome-associated neural activity in mPFC-
251 NAc and vHip-NAc modulates task engagement. To test this, we examined if neural activity at
252 ITI end predicted latency to lever press on the subsequent trial, a metric operationalizing
253 engagement (Bari et al., 2019; Beierholm et al., 2013; Cox et al., 2023; Hamid et al., 2016; Niv
254 et al., 2007). A linear mixed effects model revealed modest yet significant relationships between
255 latency to lever press and mPFC-NAc, vHip-NAc, and the interaction of mPFC-NAc and vHip-
256 NAc activity (Fig. 5A, Supplementary Table 2; Fig. S6). This suggests that increased activity
257 during outcome integration in either circuit increases latency to lever press, indicating reduced
258 behavioral engagement.
259

260 From the association between neural activity and latency, we hypothesized that reward
261 suppresses activity in mPFC-NAc and vHip-NAc to support behavioral engagement, defining a
262 mechanism whereby recent reward history modulates engagement in reward-motivated
263 behavior. We predicted that acutely increasing activity in either mPFC-NAc or vHip-NAc would
264 suppress engagement. To test this, we injected retrograding AAV-ChR2 into NAc and implanted

265 fibers above mPFC and vHip to deliver blue light stimulation during the ITI on a subset of trials
266 in the two-armed bandit task (Fig. 5B-E; Fig. S7). To test if mPFC-NAc and vHip-NAc uniquely
267 or redundantly control behavior we stimulated each circuit alone or both simultaneously.
268 Stimulating either circuit alone had no effect, whereas stimulating both simultaneously increased
269 latency to lever press, but did not alter choice behavior (Fig. 5F; Fig. S8A). This could indicate
270 either a threshold for sufficient cumulative glutamatergic drive or a requirement for synergistic
271 interaction between inputs. To differentiate these possibilities, we repeated the experiment with
272 stronger stimulation. Strong stimulation of either circuit alone increased latency to lever press,
273 again with no effect on choice (Fig. 5G, Fig. S8B). This shows that total glutamatergic input
274 modulates engagement, independent of input identity. mPFC-NAc stimulation yielded a slightly
275 weaker effect than vHip-NAc, consistent with previous findings that mPFC projections to NAc
276 medial shell are sparser than those from vHip (Britt et al., 2012). Stimulation during lever
277 presentation did not yield any changes in latency or choice behavior, supporting the importance
278 of neural integration of outcome during the ITI period, prior to action initiation (Fig. S9). Together
279 our results demonstrate that mPFC-NAc and vHip-NAc dynamically track outcome information
280 to modulate behavioral engagement according to recent history of reward. While each circuit is
281 specialized to execute this function under distinct behavioral states, once engaged, they
282 redundantly modulate behavior pointing to complementary roles in control of reward seeking.
283

284 DISCUSSION

285

286 We examined redundancy and specificity in the function of two distinct glutamatergic inputs to
287 the NAc. Using dual-site fiber photometry to probe trial-by-trial outcome encoding
288 simultaneously in two circuits in the same animal during reward-guided choice, we find that
289 mPFC-NAc and vHip-NAc similarly integrate reward via suppression of neural activity. By then
290 systematically manipulating the conditions in which outcomes are encountered, we revealed
291 that each circuit executes this common function under distinct behavioral states. While the
292 mPFC-NAc invariantly encodes outcome, vHip-NAc uses information about loss to tune
293 outcome encoding, effectively amplifying surprising reward. By comparing independent or
294 synchronous circuit-specific optogenetic stimulation we show that, once engaged, these circuits
295 cooperatively execute a shared function, i.e. modulating task engagement. Taken together, we
296 identify a redundant mechanism for outcome integration with circuit-specific gating. This
297 supports convergence of multiple inputs in tuning behavioral engagement to recent history of
298 reward.

299
300 Our finding that both mPFC-NAc and vHip-NAc integrate information about outcomes of reward-
301 motivated actions is consistent with the well-established role of mPFC in reward processing.
302 Critically, we demonstrate that this function is not specific or limited to the mPFC-NAc.
303 Globally, the mPFC encodes information about previous actions and outcomes (Sul et al., 2010)
304 and mPFC projections to the NAc bridge information about current actions and outcomes
305 across trials (Parker et al., 2022; Spellman et al., 2021). Our findings suggest these functions
306 are not unique to mPFC-NAc and are shared by vHip-NAc. However, we identify novel state
307 dependent specialization in how reward integration is engaged in each circuit. We show that the
308 mPFC-NAc fundamentally functions as a reward ledger, with reward suppressing neural activity

309 no matter the behavioral state. In contrast, we find that vHip-NAc is tuned to preferentially
310 encode outcome information after loss.

311

312 Differential encoding between mPFC-NAc and vHip-NAc emerged upon degrading task
313 requirements, a manipulation that minimizes cognitive and behavioral demands effectively
314 reducing the behavioral utility of representing integrated reward history. Under these
315 circumstances, the base functionality of each circuit is revealed: mPFC-NAc encoding is
316 anchored to reward whereas vHip-NAc is anchored to loss. Layered on top of this base
317 functionality, representation of reward history scales with task complexity in support of
318 behavioral demands. When reward is passively encountered with limited utility for action-
319 outcome associations, mPFC-NAc encoding is limited to the most recent outcome. In more
320 complex environments wherein actions elicit reward and action-outcome associations have high
321 utility, the mPFC-NAc encoding window extends to integrate reward history. In simpler task
322 structures that no longer require active engagement with a lever to earn rewards, the time-
323 constant of vHip-NAc encoding shifts such that an activity no longer increases when a single
324 unrewarded outcome follows reward. As a result, the vHip-NAc effectively comes to encode
325 consecutive loss against other outcomes. Together, this suggests a role for vHip-NAc in
326 providing information about the state of reward statistics in the environment, modulating
327 behavior as a function of loss, and revealing a novel role for this circuit as a parallel and distinct
328 stream of outcome integration.

329

330 The NAc has long been implicated in reward processing yet the precise neural circuit
331 mechanisms are still being resolved. In the NAc medial shell, reward predominantly suppresses
332 neural activity (Chen et al., 2023). This suppression likely maintains reward seeking as
333 stimulation of either D1 or D2 medium spiny neurons bidirectionally controls reward seeking
334 behavior (Lafferty et al., 2020). Here we show that reward suppresses both mPFC-NAc and
335 vHip-NAc, two major excitatory inputs to NAc medial shell. Reward-associated suppression of
336 these inputs would lead to reduced NAc activity. As such, our findings are consistent with
337 reports that optogenetic stimulation of diverse glutamatergic inputs inhibits motivated behavior
338 and the idea that glutamatergic input to NAc medial shell functions as a brake on motivated
339 behavior (Lafferty et al., 2020; Millan et al., 2017; Reed et al., 2018; Yoshida et al., 2019, 2021).
340 We show that outcome integration in mPFC-NAc and vHip-NAc initiates parallel, temporally
341 integrated, neural signaling that may engage this ‘brake’ to align ongoing behavior with recent
342 reward history and so tune behavioral engagement to prevailing environmental conditions.

343

344 Employing a redundant mechanism in mPFC-NAc and vHip-NAc may serve several functions. A
345 common mechanism makes for simple integration of multiple inputs and ensures the robustness
346 of the fundamental function of reward-guided engagement against insults. Further, modulating
347 redundant encoding with state-dependent circuit-specific sensitivity may increase the granularity
348 and range of encoding to ultimately amplify the behavioral impact of surprising rewards. We
349 demonstrate that high levels of reward suppress activity in both mPFC-NAc and vHip-NAc to
350 favor continued engagement. In contrast, strong activation of either input suppresses
351 engagement, but, when weakly activated, synchronous recruitment of both circuits is required.
352 Functionally, this may translate into a mechanism whereby moderate, balanced activity

353 predominantly modulates task engagement while allowing for strong activation of either circuit to
354 exert more direct behavioral control.

355

356 Preferential outcome encoding in vHip-NAc after loss may serve to strengthen engagement in
357 variably rewarding environments, driving increased engagement when reward is infrequently
358 encountered. The sensitivity of vHip-NAc to continuous loss, may also serve to gauge reward
359 statistics of the environment, continually increasing with each consecutive loss to trigger task
360 disengagement when activity reaches some threshold. Qualitatively, we see suggestion of this
361 in the shape of the signal after loss: mPFC-NAc tends to plateau while vHip-NAc continues to
362 increase. Ultimately, dysregulated outcome-encoding in either mPFC-NAc or vHip-NAc could
363 alter behavioral sensitivity to reward and loss. Relative to mPFC-NAc, The vHip-NAc is poised
364 to exert an outsized effect on behavioral engagement both in the strength of its input to NAc
365 medial shell (Britt et al., 2012) and in its role in signaling loss. For example, hyperactivity of
366 vHip-NAc may erroneously signal sustained loss, causing premature disengagement. Given our
367 finding that engagement is modulated by the cumulative glutamatergic input to NAc, a
368 sufficiently strong vHip-NAc signal could effectively jam any reward signal from mPFC-NAc,
369 compounding insensitivity to reward that manifests as anhedonia. Indeed, disruption of the
370 balance between NAc inputs and increased vHip-NAc drive is observed following chronic stress
371 (Bagot et al., 2015; Muir et al., 2020; Pignatelli et al., 2021; Williams et al., 2020), as well as
372 chronic alcohol (Griffin et al., 2023; Kircher et al., 2019) and cocaine intake (Barrientos et al.,
373 2018; Cahill et al., 2016; Pascoli et al., 2014; Zinsmaier et al., 2022), manipulations associated
374 with aberrant reward processing.

375

376 Here we examined the simultaneous encoding in two key neural circuits for motivated behavior.
377 By considering outcome encoding within the context of recent outcome history and behavioral
378 demands we identified a common neural mechanism of sustained temporal integration of
379 reward outcomes and reveal how the external environment differentially shapes internal
380 representations within two neural circuits. We also revealed critical circuit specificity: while
381 mPFC-NAc consistently tracks outcomes, vHip-NAc preferentially encodes outcome information
382 after loss. By illustrating the interplay of redundancy and specificity in circuit control of
383 motivated behavior we demonstrate the need to contextualize events within varied behavioral
384 states to fully understand neural encoding. Overall, our findings point to the importance of
385 balanced suppression of NAc glutamatergic inputs during outcome integration to maintain
386 reward-modulated behavioral engagement.

387

388

389 **METHODS**

390 *Animals*

391 Mice were maintained on a 12-h light-dark cycle (lights on at 7:00AM) at 22-25°C, group-housed
392 with 3-4 same-sex cage-mates with *ad libitum* access to food and water. All experimental
393 manipulations occurred during the light cycle, in accordance with guidelines of McGill
394 University's Comparative Medicine and Animal Resources Center and approved by the McGill
395 Animal Care Committee. 7-week-old male and female C57BL/6J mice were obtained from

396 Jackson Laboratories and habituated to the colony room one week prior to start of
397 manipulations. Mice were food restricted to 85% of their free-feeding body weight during
398 experimentation.

399 *Surgeries*

400 Stereotaxic surgery was performed under ketamine (100 mg/kg)/xylazine (10 mg/kg)
401 anesthesia. To achieve projection-specific GCaMP7f expression in glutamatergic NAc-projecting
402 cells, 0.3 μ l pGP-AAVrg-syn-jGCaMP7f-WPRE virus (1.85×10^{13} GC/ml; Addgene) was infused
403 into the NAc (A/P: +1.3, M/L: +/-0.60, D/V: -4.9) at a rate of 0.1 μ l per min, before raising the
404 needle to D/V: -4.7 and infusing a further 0.4 μ l virus, and allowed to diffuse for 10 min before
405 withdrawing the needle. pGP-AAV-syn-jGCaMP7f-WPRE was a gift from Douglas Kim & GENIE
406 Project (Addgene plasmid # 104488 ; <http://n2t.net/addgene:104488> ; RRID:Addgene_104488)
407 (Dana et al., 2019). Chronically implantable optic fibers (Neurophotometrics) with 200 μ m core
408 and 0.37 NA threaded through ceramic ferrules were implanted above the ventral subiculum of
409 the vHip (A/P: -3.40, M/L: +/-3.00, D/V: -4.75) and infralimbic mPFC (A/P: 1.90, M/L: +/-0.3, D/V:
410 -2.80). Recordings began minimum 4 weeks after surgery to allow sufficient time for stable and
411 robust retrograde virus expression. To achieve projection-specific ChR2 expression in
412 glutamatergic NAc-projecting cells, 0.3 μ l pGP-AAVrg-hSyn-hChR2(H134R)-EYFP virus ($7 \times$
413 10^{12} GC/ml; Addgene) or a fluorophore only control, pGP-AAVrg-hSyn-mCherry (7×10^{12} GC/ml;
414 Addgene) was infused into the NAc (A/P: +1.3, M/L: +/-0.60, D/V: -4.9) at a rate of 0.1 μ l per
415 min, before raising the needle to D/V: -4.7 and infusing a further 0.4 μ l virus, and allowed to
416 diffuse for 10 min before withdrawing the needle. pAAV-hSyn-hChR2(H134R)-EYFP was a gift
417 from Karl Deisseroth (Addgene plasmid # 26973; <http://n2t.net/addgene:26973> ;
418 RRID:Addgene_26973). pAAV-hSyn-mCherry was a gift from Karl Deisseroth (Addgene plasmid
419 # 114472; <http://n2t.net/addgene:114472> ; RRID:Addgene_114472). Chronically implantable
420 optic fibers (Neurophotometrics) with 200 μ m core and 0.22 NA threaded through ceramic
421 ferrules were implanted above the ventral subiculum of the vHip (A/P: -3.40, M/L: +/-3.00, D/V: -
422 4.75) and infralimbic mPFC (A/P: 1.90, M/L: +/-0.3, D/V: -2.80). Optogenetic manipulations
423 began minimum 4 weeks after surgery to allow sufficient time for stable and robust retrograde
424 virus expression.

425 *Histology*

426 After completion of all behavioral testing, mice were deeply anesthetized with ketamine/xylazine
427 and transcardially perfused with phosphate buffered saline (PBS) and paraformaldehyde (4%).
428 Brains were removed and post-fixed in paraformaldehyde for 24h and stored in PBS until
429 sectioning on a vibratome (50 μ m). Sections were mounted with Vectashield with DAPI (Vector
430 Laboratories) and examined under a fluorescent microscope (Leica DM6000 B) to confirm viral
431 expression and fiber placement. A confocal microscope (Zeiss LSM800) was used to obtain
432 fluorescent images. Images were acquired as tiles with a 20x air objective (NA 0.8) using Zeiss
433 Zen Blue imaging software. Images were collected in the McGill University Advanced
434 Bioluminescence Facility (ABIF), RRID:SCR_017697. Mistargeted animals were excluded from
435 analysis.

436 *Apparatus*

437 Behavioral experiments were performed in standard Med Associates operant boxes (15.24 x
438 13.34 x 12.7 cm) enclosed in sound attenuating chambers outfitted with a programmable audio
439 generator, two retractable levers and cue lights either side of a food port for delivering a liquid
440 chocolate milk reward (30µl, Nesquik) diluted with water in a 2:1 ratio. Boxes were controlled
441 and data collected by a computer running MED-PC software (Med-Associates).

442 *Lever Press Training*

443 Training was completed in three stages, with all training sessions lasting 30 minutes. In the first
444 stage, animals were presented with two levers, both of which delivered a chocolate milk reward
445 with a 100% probability. To signal the start of the trial, both levers extended and the cue lights
446 above the levers turned on, animals then had 60 seconds to make a response on either lever. A
447 press on either lever resulted in lever retraction, immediate delivery of a 30 µL chocolate milk
448 reward, and the start of a 3 second auditory cue (2kHz pure tone or white noise). Following
449 either a lever press or 60 seconds with no press (i.e. an omission), a 10 second intertrial interval
450 (ITI) was triggered. After one session with over 25 responses, animals progressed to the second
451 stage. In this stage animals again were presented with two levers but reward was now delivered
452 with a 50% probability on both levers. To signal the start of the trial, both levers extended and
453 the cue lights above the levers turned on, animals then had 60 seconds to make a response. A
454 lever press resulted in lever retraction and immediate delivery of the outcome, either a 30 µL
455 chocolate milk reward and a 3 second auditory cue (2kHz pure tone or white noise,
456 counterbalanced across animals) or just a 3 second auditory cue (white noise or 2kHz pure
457 tone). Following either a lever press or omission, a 10 second intertrial interval (ITI) was
458 triggered. Following two consecutive sessions with over 40 responses, animals progressed to
459 the third stage. This stage was the same as stage two except that animals now had only 10
460 seconds to make a response before an omission was registered. Following two consecutive
461 sessions with over 100 responses animals achieved criterion to progress to the two-armed
462 bandit task.

463 *Two-armed bandit Task*

464 The two-armed bandit task was performed over of 6 days with each session lasting one hour. In
465 this task, animals were presented with two levers with one lever rewarded on 80% of trials, and
466 the other lever rewarded on 20% of trials. To signal the start of the trial, both levers extended
467 and the cue lights above the levers turned on, animals then had 10 seconds to make a
468 response on either lever or an omission was registered. A lever press resulted in lever retraction
469 and immediate delivery of the outcome, either a 30 µL chocolate milk reward and a 3 second
470 auditory cue (2kHz pure tone or white noise, counterbalanced across animals) or simply a
471 different 3 second auditory cue (white noise or 2kHz pure tone) signaling non-reward. Following
472 either a lever press or an omission, a 10 second intertrial interval (ITI) was triggered. To
473 maintain a dynamic learning environment and high rates of rewarded and unrewarded
474 outcomes, probability of reward was switched between levers after five consecutive responses
475 on the high probability lever. Four males and four females remained on the two-armed bandit
476 task during the task degradation (data not shown).

477 *One-Lever Forced Choice Task*

478 The one lever forced choice task was performed over 3 days with each session lasting one
479 hour. In this task, animals were presented with a single lever (counterbalanced across animals).
480 Pressing this lever resulted in probabilistic reward on a predetermined schedule. The outcome
481 schedule was matched to each animal's individual performance in the final three days of the
482 two-armed bandit task, such that the first session in the one-lever task was yoked to the reward
483 schedule experienced by the animal on day four in the two-armed bandit task, the second to day
484 five, and the third to day six. To signal the start of the trial, the lever extended and the cue light
485 above the lever turned on. Animals then had 10 seconds to make a response. A lever press
486 resulted in lever retraction and immediate delivery of the outcome, either a 30 μ L chocolate milk
487 reward and a 3 second auditory cue (2kHz pure tone or white noise) or simply a different 3
488 second auditory cue (white noise or 2kHz pure tone). Following either a lever press or an
489 omission, a 10 second intertrial interval (ITI) was triggered.

490 *No Lever Response Free Task*

491 The no lever response free task was performed over the course of 3 days with each session
492 lasting one hour. In this task, animals were able to retrieve non-contingently delivered rewards
493 under a similar trial structure to both the two-armed bandit task and the one-lever forced choice
494 task but with no levers available. To signal the start of the trial, cue lights above both levers
495 turned on and remained illuminated for a period of time matched to each animal's response time
496 in the last three days of the two-armed bandit task. After cue lights turned off, outcomes were
497 delivered, either a 30 μ L chocolate milk reward and a 3 second auditory cue (2kHz pure tone or
498 white noise) or simply a different 3 second auditory cue (white noise or 2kHz pure tone). As in
499 the one-lever task, the outcome schedule was matched to each animal's performance in the
500 final three days of the two-armed bandit task now also matching the latency to receive the
501 outcome to the trial-by-trial latency to lever press on the two-armed bandit task with a 10 second
502 intertrial interval (ITI).

503 *Frame Independent Projected Fiber Photometry*

504 To measure calcium-associated changes in fluorescence in real time, recordings were made
505 from vHip-NAc and mPFC-NAc-projecting cells during the two-armed bandit task, the one-lever
506 forced choice task, and the no lever response free task. Samples were collected at a frequency
507 of 20 Hz using Neurophotometrics hardware through Bonsai and FlyCap software. Recordings
508 were coupled to the start of behavioral analysis by interfacing Bonsai with MED-PC using a
509 custom DAQ box (Neurophotometrics).

510 *Photometry data extraction and normalization*

511 *Photometry data* were extracted and analyzed using custom-written scripts in Python. To
512 normalize the data, the control channel (415nm) was fitted to the raw (470nm). The fitted control
513 was then subtracted from the raw trace. The resultant trace was divided by the fitted control
514 giving the $\Delta F/F$ and converted to a Z-score. This calculation was performed over the entirety of
515 the session to preserve dynamic fluctuation in population activity that persists beyond individual
516 trials to allow comparison across trials. For heatmaps Z-scores were baseline subtracted from

517 average activity in the two seconds prior to lever press to accommodate moving baselines. For
518 analyses of reward history, Z-scores were baseline subtracted from average activity in the two
519 seconds prior to lever press on trial t-1 to account for shifted baselines in trial t0.

520 *Optogenetics in Two-armed Bandit Task*

521 Following lever press training, animals started the two-armed bandit task with optogenetic
522 manipulations of mPFC-NAc and vHip-NAc activity for the duration of the ITI. Each day animals
523 received either mPFC-NAc, vHip-NAc, or simultaneous mPFC-NAc and vHip-NAc stimulation on
524 a subset of trials over the course of 9 days such that they received a total of 3 days of
525 stimulation per condition for each stimulation protocol tested (5 Hz, 10 ms, 1-2 mW; 8 Hz, 10
526 ms, 2-3 mW). Order of stimulation days was fully counterbalanced within and between mice to
527 avoid any order effects. Stimulation was delivered by 450 nm lasers controlled by a laser driver
528 (Doric) running Doric studios software and triggered via a TTL (Med-Associates) at ITI start on a
529 random subset of trials (30%) and terminated immediately prior to lever extension.

530 *Ex vivo current-clamp electrophysiology*

531 Brain slice preparation

532 Mice were deeply anesthetized with isofluorane. Transcardial perfusion was performed with 25-
533 30 ml of ice-chilled carbogenated NMDG artificial cerebrospinal fluid (aCSF: containing in mM:
534 92 NMDG, 2.5 KCl, 1.25 NaH₂PO₄, 30 NaHCO₃, 20 HEPES, 25 glucose, 2 thiourea, 5 Na-
535 ascorbate, 3 Na-pyruvate, 0.5 CaCl₂·4H₂O and 10 MgSO₄·7H₂O; titrated to pH 7.3–7.4 with
536 concentrated hydrochloric acid). Brain slices (200 µm) were prepared in ice-chilled
537 carbogenated NMDG aCSF by a vibratome (Lecia VT 1200S). All brain slices were recovery in
538 32–34 °C carbogenated NMDG aCSF for 10 min and then were transferred into room-
539 temperature carbogenated HEPES holding aCSF (containing in mM: 92 NaCl, 2.5 KCl, 1.25
540 NaH₂PO₄, 30 NaHCO₃, 20 HEPES, 25 glucose, 2 thiourea, 5 Na-ascorbate, 3 Na-pyruvate, 2
541 CaCl₂·4H₂O and 2 MgSO₄·7H₂O; titrated to pH to 7.3–7.4 with NaOH) for at least 1 hour before
542 current-clamp recording.

543 Electrophysiology recordings

544 Current-clamp recordings were performed in room-temperature carbogenated aCSF (containing
545 in mM: mM: 128 NaCl, 3 KCl, 1.25 NaH₂PO₄, 2 MgCl₂, 2 CaCl₂, 24 NaHCO₃ and 10 glucose; pH
546 7.2). The patch pipette solution was composed of (in mM) 115 K-gluconate, 20 KCl, 1.5 MgCl₂,
547 10 Phosphocreatine-Tris, 2 Mg-ATP, 0.54 Na-GTP and 10 HEPES. Blue light (wavelength: 470
548 nm) from a LED system (DC4100, Thorlabs) was used for optogenetic stimulation to evoke
549 action potentials. The optogenetic stimulation protocol consisted of trains of 5 Hz (1-2 mW) or 8
550 Hz (2-3 mW) 10ms light pulses for 5 s. All signals were amplified and digitized by Multiclamp
551 700B (Molecular Device) and Digidata 1550B (Molecular Device) respectively. Series and
552 access resistance were monitored during the experiments and signals were bessel filtered at 2
553 kHz.

554 *Data Analysis & Statistics*

555 Linear Mixed Effects Regression

556 Linear Mixed Effects Regression Models are a powerful approach to probe variance attributable
557 to variables of interest (e.g. trial outcome) while simultaneously controlling for random effects
558 (e.g. session ID) (Fetcho et al., 2023; Kato et al., 2022; Yu et al., 2022). This is useful for
559 modeling instances where there is nonindependence in the structure of data e.g. multiple trials
560 recorded within multiple animals. Models were fit using the full interaction of the factors of
561 interest (trial outcome, previous trial outcome, sex) and using animal ID and session ID as
562 random effects using the *lme4* package in R (Bates et al., 2014). Where the dependent variable
563 was latency, a Gamma link function was used to approximate the non-gaussian distribution. The
564 fitted models were used to calculate estimated marginal means using the *emmeans* package in
565 R (Lenth et al., 2021). The effect of variables of interest were then examined by comparing
566 estimated marginal means. Given the large number of samples generated using this approach
567 (all trials x all animals), comparisons of estimated marginal means were conducted using a Z-
568 test and Sidak's method to adjust for multiple comparisons.

569 Cross-Correlation Time Delay Analysis

570 Time delay analysis was performed by first calculating the cross-correlation between mPFC-
571 NAc and vHip-NAc during the ITI across a maximum lag of \pm 5 seconds using the CCF function
572 in R. The argument of the maximum (i.e. the time offset of peak correlation) of the resulting
573 cross-correlation function was used to estimate the delay between mPFC-NAc and vHip-NAc on
574 a trial-by-trial basis (Abboud & Sadeh, 1984). Linear mixed effects models were then fit to
575 assess if the delay was non-zero (i.e. non-synchronous) using the following models to test for
576 effects of sex [Time Delay~Sex-1+(1|ID)+(1|Day)] and for the interaction between sex and
577 reward [Time Delay~Rewards:Sex-1+(1|ID)+(1|Day)]. The resulting regression coefficients from
578 each model were examined to determine if the time delay was non-zero in any group (i.e.
579 regression coefficient significantly different from zero).

580
581 Conditional Entropy Analysis
582

583 Conditional entropy is an information measure used to estimate the amount of additional
584 information needed to explain one signal given full knowledge of a second signal. This can be
585 interpreted as the unique information contributed by a second signal beyond that contributed by
586 a first with smaller conditional entropy suggesting less unique information carried by the second
587 signal. Conditional entropy was calculated on the first two seconds and the last two seconds of
588 the ITI using the PyInform package in Python to calculate the entropy (\square) of the mPFC circuit
589 given the vHip-NAc circuit, $\square(mPFC-NAc|vHip-NAc)$, and the entropy of the vHip-NAc circuit
590 given the mPFC-NAc circuit, $\square(vHip-NAc|mPFC-NAc)$ (Cover & Thomas, 1991; Moore et al.,
591 2018).

592
593 Code Availability
594

595 Code used to perform analyses for all figures available at
596 https://github.com/eshaaniyer/mPFCvHip-NAc_RewardIntegration

597
598 **ACKNOWLEDGMENTS**

599

600 We would like to thank Dr. Becket Ebitz, Dr. Mihaela Iordanova and Heike Schuler for their
601 helpful comments and feedback throughout this project. Renderings of mice were created with
602 BioRender.com. Research was supported by grants to RCB from NSERC and the Ludmer
603 Centre for Neuroinformatics and Mental Health.

604

605 **Author contributions**

606

607 Conceptualization, E.S.I and R.C.B.; Methodology, E.S.I and R.C.B.; Investigation, E.S.I, P.V.,
608 S.W., J.M., Y.C.T., V.C.; Writing – Original Draft, E.S.I and R.C.B.; Writing – Review & Editing,
609 E.S.I. and R.C.B.; Funding Acquisition, R.C.B.; Resources, R.C.B.; Supervision, R.C.B.

610

611 **Declaration of interests**

612

613 The authors declare no competing interests.

614

615 **Figures**

616

617 **Figure 1. mPFC-NAc and vHip-NAc similarly encode reward in a probabilistically**
618 **rewarded environment.** (A) Schematic of two-armed bandit task. Mice lever press in a two
619 lever task in which one lever is rewarded with chocolate milk on 80% of trials, and the other on
620 20%. Following a lever press, levers retract, and auditory cues signal outcome and start of a 10
621 sec inter-trial interval (ITI). Contingencies switch after five consecutive responses on the high
622 probability lever. Female (n=10) and male (n=12) mice robustly engage with the task,
623 experiencing similar numbers of (B) unrewarded (C) rewarded and (D) omission trials. (E)
624 Retrograding jGCaMP7f is injected into the nucleus accumbens (NAc) and optic fibers
625 implanted in medial prefrontal cortex (mPFC) and ventral hippocampus (vHip) to simultaneously
626 probe neural activity indicated by Ca^{2+} -associated fluorescence changes in (F) mPFC neurons
627 projecting to NAc (mPFC-NAc) and (G) vHip neurons projecting to NAc (vHip-NAc) as mice
628 encounter reward and non-reward. Estimated mean mPFC-NAc activity across all rewarded and
629 unrewarded trials in (H) female (n=10) and (I) male (n=12) mice. Analysis focused on 8-10 sec
630 after lever press (ITI end). At ITI end, mPFC-NAc activity is suppressed by rewarded outcomes
631 in female (J; $Z=21.348$, $p<0.0001$) and male (K; $Z=19.625$, $p<0.0001$) mice. Estimated mean
632 vHip-NAc activity across all rewarded and unrewarded trials in (L) female and (M) male mice. At
633 ITI end, vHip-NAc activity is suppressed by rewarded outcomes in female (N; $Z=8.161$;
634 $p<0.0001$) and male (O; $Z=8.924$; $p<0.0001$) mice. Heatmap of mPFC-NAc activity to (P)
635 rewarded outcomes and (Q) unrewarded outcomes in a representative animal across one
636 session. Heatmap of vHip-NAc activity to (R) rewarded outcomes and (S) unrewarded outcomes
637 in a representative animal across one session. Error bars represent SEM around the estimated
638 mean. **** $p<0.0001$

639

640 **Figure 2. mPFC-NAc and vHip-NAc similarly integrate reward history.** (A) Estimated mean
641 mPFC-NAc activity across pairs of consecutive trials ($t-1 \rightarrow t0$) showing rewarded+rewarded
642 (R→R), rewarded+unrewarded (R→U), unrewarded+rewarded (U→R), and

643 unrewarded+unrewarded (U→U) trial pairs in female (n=10) and male (n=12) mice. Analysis
644 focused on 8-10 sec after lever press (ITI end). (B) On trial t-1, mPFC-NAc activity is
645 significantly suppressed by reward (U→U vs R→U: $Z=28.99496$, $p<0.0001$; U→R vs R→R:
646 $Z=25.6767$, $p<0.0001$). (C) On the subsequent trial, t0, mPFC-NAc activity is significantly
647 suppressed by current reward (U→U vs U→R: $Z=-28.5098$, $p<0.0001$; R→U vs R→R: $Z=-$
648 19.8981 , $p<0.0001$). When trial t0 is unrewarded, mPFC-NAc activity remains significantly
649 suppressed by reward experienced on the previous trial, t-1, (U→U vs R→U: $Z= 9.19653$,
650 $p<0.0001$). (D) Estimated mean vHip-NAc activity across pairs of consecutive trials (t-1→t0)
651 showing rewarded+rewarded (R→R), rewarded+unrewarded (R→U), unrewarded+rewarded
652 (U→R), and unrewarded+unrewarded (U→U) trial pairs. (E) On trial t-1, vHip-NAc activity is
653 significantly suppressed by reward (U→U vs R→U: $Z=14.9372$, $p<0.0001$; U→R vs R→R:
654 $Z=11.6962$, $p<0.0001$). (F) On the subsequent trial, t0, vHip-NAc activity is significantly
655 suppressed by current reward (U→U vs U→R: $Z=-17.4993$, $p<0.0001$; U→U vs R→R: $Z=-$
656 7.1005 , $p<0.0001$). When trial t0 is unrewarded, vHip-NAc activity remains suppressed by
657 reward experienced on the previous trial, t-1, (U→U vs R→U: $Z= 11.4112$, $p<0.0001$).
658 Individual-animal averages are indicated by circles for males and triangles for females. Error
659 bars represent SEM around the estimated mean. **** $p<0.0001$

660

661 **Figure 3. mPFC-NAc and vHip-NAc are differentially sensitive to loss.** (A) Venn diagram
662 representing the relationship between the mutual information and conditional entropy that exists
663 between observed mPFC-NAc and vHip-NAc signals. Conditional entropy is a measure of the
664 additional unique information contributed by a second signal given fully knowledge of a first
665 signal. (B) Conditional entropy in mPFC-NAc is reduced on rewarded relative to unrewarded
666 trials regardless of previous outcome (U→U vs U→R: $Z=2.8644$, $p<0.0001$; R→U vs R→R:
667 $Z=3.5185$, $p<0.0001$) indicating that less unique information is carried in mPFC-NAc after
668 reward. (C) Conditional entropy in vHip-NAc is increased on rewarded relative to unrewarded
669 trials only when the prior outcome was unrewarded (U→U vs U→R: $Z=-3.7566$, $p=0.0003$)
670 indicating that more unique information is carried in vHip-NAc when reward follows nonreward.
671 Comparison of activity at ITI end on currently rewarded or unrewarded trials considering prior
672 outcome history up to three trials back shows that (D) mPFC-NAc activity is suppressed on
673 every currently rewarded trial indicating that mPFC-NAc consistently encodes current outcome
674 via relative suppression regardless of outcome history. In contrast, (E) vHip-NAc activity is
675 suppressed on currently rewarded trials except when current reward is preceded by two
676 ($Z=1.2310$, $p=0.8606$) or three ($Z=0.8398$, $p=0.9834$) prior consecutive rewards indicating that
677 vHip-NAc ceases to encode current outcome via relative suppression after consistent reward.
678 See supplementary table 29 for all comparisons. Error bars represent SEM around the
679 estimated mean. * $p<0.05$, ** $p<0.001$, **** $p<0.0001$

680

681 **Figure 4. Degrading task requirements reveals circuit specialization in integrating reward**
682 **history.** (A) Schematic of one-lever forced choice task in which lever presses are rewarded on
683 a schedule yoked to each animal's individual performance in the final three days of the two-
684 armed bandit task. Following a lever press, levers retract, and auditory cues signal outcome and
685 start of a 10 sec inter-trial interval (ITI). (B) Estimated mean mPFC-NAc activity across pairs of
686 consecutive trials (t-1→t0) showing rewarded+rewarded (R→R), rewarded+unrewarded

687 (R→U), unrewarded+rewarded (U→R), and unrewarded+unrewarded (U→U) trial pairs (male
688 n= 8, female n=6). Analysis focused on 8-10 sec after lever press (ITI end). (C) On trial t0,
689 mPFC-NAc activity is suppressed by reward (U→U vs U→R: Z=18.8757, p<0.0001; R→U vs
690 R→R: Z=12.0687, p<0.0001). When trial t0 is unrewarded, mPFC-NAc activity remains
691 suppressed by reward experienced on the previous trial, t-1, (U→U vs R→U: Z= 6.3467,
692 p<0.0001). (D) Estimated mean vHip-NAc activity across pairs of consecutive trials (t-1→t0)
693 showing R→R, R→U, U→R, and U→U trial pairs (male n= 8, female n=6). (E) On trial t0, vHip-
694 NAc activity is suppressed by reward (U→U vs U→R: Z=8.5245, p<0.0001; R→U vs R→R:
695 Z=4.0519, p=0.0001). When trial t0 is unrewarded, mPFC-NAc activity remains suppressed by
696 reward experienced on the previous trial, t-1, (U→U vs R→U: Z= 6.2425, p<0.0001). (F)
697 Schematic of no lever response free task. Mice are allowed to collect rewards delivered on a
698 schedule yoked to each animal's individual trial statistics (latency and outcome) of the two-
699 armed bandit task. Trial structure is signaled by cue-light illumination and after a predetermined
700 delay auditory cues signal outcome and start of a 10 sec ITI. (G) Estimated mean mPFC-NAc
701 activity across pairs of consecutive trials (t-1→t0) showing R→R, R→U, U→R, and U→U trial
702 pairs (male n= 8, female n=6). (H) On trial t0, mPFC-NAc activity is suppressed by reward
703 (U→U vs U→R: Z=8.2136, p<0.0001; R→U vs R→R: Z=7.4647, p<0.0001). (I) Estimated mean
704 vHip-NAc activity across pairs of consecutive trials (t-1→t0) showing R→R, R→U, U→R, and
705 U→U trial pairs (male n= 8, female n=6). (J) On trial t0, vHip-NAc activity is suppressed by
706 reward only if trial t-1 was unrewarded (U→U vs U→R: Z=3.7413, p=0.0003). When trial t0 is
707 unrewarded, vHip-NAc activity remains suppressed by reward experienced on the previous trial,
708 t-1, (U→U vs R→U: Z= 3.8661, p=0.0002). Individual-animal averages are indicated by circles
709 for males and triangles for females. Error bars represent SEM around the estimated mean.
710 ***p<0.001, ****p<0.0001
711

712 **Figure 5. mPFC-NAc and vHip-NAc modulate task engagement.** (A) Heatmap of estimated
713 latency to respond on the subsequent trial given mPFC-NAc and vHip-NAc activity at ITI end
714 shows that increased activity associates with longer latency. (B) Optogenetic stimulation in the
715 two-armed bandit task is delivered for the duration of the ITI to either mPFC-NAc, vHip-NAc, or
716 simultaneously to both circuits. (C) AAVrg-ChR2-mCherry or AAVrg-mCherry is injected into the
717 NAc and optic fibers implanted in mPFC and vHip to stimulate (D) mPFC-NAc neurons and (E)
718 vHip-NAc neurons. (F) Simultaneous 5Hz stimulation of mPFC-NAc and vHip-NAc, but neither
719 circuit individually, increased latency to respond in ChR2 animals (male n=6, female n=7)
720 compared to mCherry controls (male n=6, female n=6; Z=-18.6984, p<0.0001). (G) 8 Hz
721 stimulation of mPFC-NAc (Z=-12.6970, p=0.01354), vHip-NAc (Z=-23.8073, p<0.0001), and
722 simultaneous stimulation of both mPFC-NAc and vHip-NAc (Z=-24.1357, p<0.0001) all
723 increased latency in ChR2 animals (male n= 5, female n=6) compared to mCherry controls
724 (male n= 6, female n=6). Individual-animal averages are indicated by circles for males and
725 triangles for females. Error bars represent SEM around the estimated mean.
726 **p<0.01, ****p<0.0001
727

728

729 REFERENCES

730

731 **A1**boud, S., & Sadeh, D. (1984). The use of cross-correlation function for the alignment of ECG
732 waveforms and rejection of extrasystoles. *Computers and Biomedical Research*, 17(3), 258–
733 266. [https://doi.org/10.1016/S0010-4809\(84\)80017-8](https://doi.org/10.1016/S0010-4809(84)80017-8)

734 **B1**agot, R. C., Parise, E. M., Peña, C. J., Zhang, H.-X., Maze, I., Chaudhury, D., Persaud, B., Cachope,
735 R., Bolaños-Guzmán, C. A., Cheer, J. F., Deisseroth, K., Han, M.-H., & Nestler, E. J. (2015).
736 Ventral hippocampal afferents to the nucleus accumbens regulate susceptibility to depression.
737 *Nature Communications*, 6, 7062. <https://doi.org/10.1038/ncomms8062>

738 **B2**ai, B. A., Grossman, C. D., Lubin, E. E., Rajagopalan, A. E., Cressy, J. I., & Cohen, J. Y. (2019).
739 Stable representations of decision variables for flexible behavior. *Neuron*, 103(5), 922-933.e7.
740 <https://doi.org/10.1016/j.neuron.2019.06.001>

741 **B3**arker, J. M., Bryant, K. G., & Chandler, L. J. (2019). Inactivation of ventral hippocampus projections
742 promotes sensitivity to changes in contingency. *Learning & Memory*, 26(1), 1–8.

743 **B4**rientos, C., Knowland, D., Wu, M. M. J., Lilascharoen, V., Huang, K. W., Malenka, R. C., & Lim, B.
744 K. (2018). Cocaine-Induced Structural Plasticity in Input Regions to Distinct Cell Types in
745 Nucleus Accumbens. *Biological Psychiatry*, 84(12), 893–904.
746 <https://doi.org/10.1016/j.biopsych.2018.04.019>

747 **B5**ates, D., Mächler, M., Bolker, B., & Walker, S. (2014). Fitting linear mixed-effects models using lme4.
748 *arXiv Preprint arXiv:1406.5823*.

749 **B6**erholm, U., Guitart-Masip, M., Economides, M., Chowdhury, R., Düzel, E., Dolan, R., & Dayan, P.
750 (2013). Dopamine Modulates Reward-Related Vigor. *Neuropsychopharmacology*, 38(8), 1495–
751 1503. <https://doi.org/10.1038/npp.2013.48>

752 **B7**olger, J. P., Benaliouad, F., McDevitt, R. A., Stuber, G. D., Wise, R. A., & Bonci, A. (2012). Synaptic and
753 Behavioral Profile of Multiple Glutamatergic Inputs to the Nucleus Accumbens. *Neuron*, 76(4),
754 790–803. <https://doi.org/10.1016/j.neuron.2012.09.040>

755 **B8**oill, M. E., Bagot, R. C., Gancarz, A. M., Walker, D. M., Sun, H., Wang, Z.-J., Heller, E. A., Feng, J.,
756 Kennedy, P. J., Koo, J. W., Cates, H. M., Neve, R. L., Shen, L., Dietz, D. M., & Nestler, E. J.
757 (2016). Bidirectional Synaptic Structural Plasticity after Chronic Cocaine Administration Occurs
758 through Rap1 Small GTPase Signaling. *Neuron*, 89(3), 566–582.
759 <https://doi.org/10.1016/j.neuron.2016.01.031>

760 **B9**oter, A. G., Soler-Llavina, G. J., & Sabatini, B. L. (2007). Timing and Location of Synaptic Inputs
761 Determine Modes of Subthreshold Integration in Striatal Medium Spiny Neurons. *The Journal of
762 Neuroscience*, 27(33), 8967–8977. <https://doi.org/10.1523/JNEUROSCI.2798-07.2007>

763 **B10**en, G., Lai, S., Bao, G., Ke, J., Meng, X., Lu, S., Wu, X., Xu, H., Wu, F., Xu, Y., Xu, F., Bi, G.-Q.,
764 Peng, G., Zhou, K., & Zhu, Y. (2023). Distinct reward processing by subregions of the nucleus
765 accumbens. *Cell Reports*, 42(2). <https://doi.org/10.1016/j.celrep.2023.112069>

766 **B11**istoffel, D. J., Walsh, J. J., Hoerbelt, P., Heifets, B. D., Llorach, P., Lopez, R. C., Ramakrishnan, C.,
767 Deisseroth, K., & Malenka, R. C. (2021). Selective filtering of excitatory inputs to nucleus
768 accumbens by dopamine and serotonin. *Proceedings of the National Academy of Sciences*,
769 118(24), e2106648118. <https://doi.org/10.1073/pnas.2106648118>

770 **B12**over, T. M., & Thomas, J. A. (1991). Entropy, relative entropy and mutual information. *Elements of
771 Information Theory*, 2(1), 12–13.

770, J., Minerva, A. R., Fleming, W. T., Zimmerman, C. A., Hayes, C., Zorowitz, S., Bandi, A., Ornelas,
773 S., McMannon, B., Parker, N. F., & Witten, I. B. (2023). A neural substrate of sex-dependent
774 modulation of motivation. *Nature Neuroscience*, 26(2), Article 2. <https://doi.org/10.1038/s41593-022-01229-9>

775

776 Ma, H., Sun, Y., Mohar, B., Hulse, B. K., Kerlin, A. M., Hasseman, J. P., Tsegaye, G., Tsang, A.,
777 Wong, A., Patel, R., Macklin, J. J., Chen, Y., Konnerth, A., Jayaraman, V., Looger, L. L.,
778 Schreiter, E. R., Svoboda, K., & Kim, D. S. (2019). High-performance calcium sensors for
779 imaging activity in neuronal populations and microcompartments. *Nature Methods*, 16(7), 649–
780 657. <https://doi.org/10.1038/s41592-019-0435-6>

781 Cho, R. N., Hall, B. S., Estrin, D. J., Walsh, A. P., Schuette, P. J., Kaminsky, J., Singh, A.,
782 Roshgodal, J., Bavley, C. C., Nadkarni, V., Antigua, S., Huynh, T. N., Grosenick, L., Carthy, C.,
783 Komer, L., Adhikari, A., Lee, F. S., Rajadhyaksha, A. M., & Liston, C. (2023). Regulation of
784 social interaction in mice by a frontostriatal circuit modulated by established hierarchical
785 relationships. *Nature Communications*, 14, 2487. <https://doi.org/10.1038/s41467-023-37460-6>

786 Floresco, S. B. (2015). The Nucleus Accumbens: An Interface Between Cognition, Emotion, and Action.
787 *Annual Review of Psychology*, 66(1), 25–52. <https://doi.org/10.1146/annurev-psych-010213-115159>

788

789 French, S. J., & Totterdell, S. (2002). Hippocampal and prefrontal cortical inputs monosynaptically
790 converge with individual projection neurons of the nucleus accumbens. *Journal of Comparative
791 Neurology*, 446(2), 151–165.

792 Ganbari, M., Li, G., Hsu, L., & Yap, P. (2023). Accumulation of network redundancy marks the early
793 stage of Alzheimer's disease. *Human Brain Mapping*, 44(8), 2993–3006.
794 <https://doi.org/10.1002/hbm.26257>

795

796 Gace, A. A., Floresco, S. B., Goto, Y., & Lodge, D. J. (2007). Regulation of firing of dopaminergic
797 neurons and control of goal-directed behaviors. *Trends in Neurosciences*, 30(5), 220–227.
798 <https://doi.org/10.1016/j.tins.2007.03.003>

799

800 Gaffin, W. C., Lopez, M. F., Woodward, J. J., & Becker, H. C. (2023). Alcohol dependence and the
801 ventral hippocampal influence on alcohol drinking in male mice. *Alcohol*, 106, 44–54.
802 <https://doi.org/10.1016/j.alcohol.2022.10.004>

803

804 Hamel, L., Cavdaroglu, B., Yeates, D., Nguyen, D., Riaz, S., Patterson, D., Khan, N., Kirolos, N.,
805 Roper, K., Ha, Q. A., & Ito, R. (2022). Cortico-Striatal Control over Adaptive Goal-Directed
806 Responding Elicited by Cues Signaling Sucrose Reward or Punishment. *Journal of
807 Neuroscience*, 42(18), 3811–3822. <https://doi.org/10.1523/JNEUROSCI.2175-21.2022>

808

809 Hamed, A. A., Pettibone, J. R., Mabrouk, O. S., Hetrick, V. L., Schmidt, R., Vander Weele, C. M.,
810 Kennedy, R. T., Aragona, B. J., & Berke, J. D. (2016). Mesolimbic Dopamine Signals the Value
811 of Work. *Nature Neuroscience*, 19(1), 117–126. <https://doi.org/10.1038/nn.4173>

812

813 Matani, N., & Fukai, T. (2018). Redundancy in synaptic connections enables neurons to learn
814 optimally. *Proceedings of the National Academy of Sciences*, 115(29), E6871–E6879.
815 <https://doi.org/10.1073/pnas.1803274115>

816

817 Matsumoto, T., Mitsukura, Y., Yoshida, K., Mimura, M., Takata, N., & Tanaka, K. F. (2022). Oscillatory
818 Population-Level Activity of Dorsal Raphe Serotonergic Neurons Is Inscribed in Sleep Structure.
819 *The Journal of Neuroscience*, 42(38), 7244–7255. <https://doi.org/10.1523/JNEUROSCI.2288-21.2022>

815 Sher, D. M., Aziz, H., Mangieri, R. A., & Morrisett, R. A. (2019). Ethanol Experience Enhances
816 Glutamatergic Ventral Hippocampal Inputs To D1 Receptor-Expressing Medium Spiny Neurons
817 In The Nucleus Accumbens Shell. *The Journal of Neuroscience*, 3051–18.
818 <https://doi.org/10.1523/JNEUROSCI.3051-18.2019>

819 Fertig, C. K., Yang, A. K., Mendoza, J. A., & Britt, J. P. (2020). Nucleus Accumbens Cell Type- and
820 Input-Specific Suppression of Unproductive Reward Seeking. *Cell Reports*, 30(11), 3729–
821 3742.e3. <https://doi.org/10.1016/j.celrep.2020.02.095>

822 Roth, R. V., Buerkner, P., Herve, M., Love, J., Riebl, H., & Singmann, H. (2021). *Emmeans: Estimated
823 marginal means, aka least-squares means. CRAN*.

824 H, E. B., Sweis, B. M., Asp, A. J., Esguerra, M., Silvis, K. A., David Redish, A., & Thomas, M. J.
825 (2023). A quadruple dissociation of reward-related behaviour in mice across excitatory inputs to
826 the nucleus accumbens shell. *Communications Biology*, 6(1), Article 1.
827 <https://doi.org/10.1038/s42003-023-04429-6>

828 Denbach, D., Vacca, G., Ahn, S., Seamans, J. K., & Phillips, A. G. (2022). Optogenetic modulation of
829 glutamatergic afferents from the ventral subiculum to the nucleus accumbens: Effects on
830 dopamine function, response vigor and locomotor activity. *Behavioural Brain Research*, 434,
831 114028. <https://doi.org/10.1016/j.bbr.2022.114028>

832 Forder, E. (2011). Variability, compensation, and modulation in neurons and circuits. *Proceedings of
833 the National Academy of Sciences of the United States of America*, 108(Suppl 3), 15542–
834 15548. <https://doi.org/10.1073/pnas.1010674108>

835 Forder, E., & Goaillard, J.-M. (2006). Variability, compensation and homeostasis in neuron and network
836 function. *Nature Reviews Neuroscience*, 7(7), 563–574. <https://doi.org/10.1038/nrn1949>

836 Yan, E. Z., Kim, H. A., & Janak, P. H. (2017). Optogenetic activation of amygdala projections to
837 nucleus accumbens can arrest conditioned and unconditioned alcohol consummatory behavior.
838 *Neuroscience*, 360, 106–117. <https://doi.org/10.1016/j.neuroscience.2017.07.044>

839 Matsuki, B. E. P., & O'Donnell, C. (2021). Neural circuit function redundancy in brain disorders.
840 *Current Opinion in Neurobiology*, 70, 74–80. <https://doi.org/10.1016/j.conb.2021.07.008>

841 Bore, D. G., Valentini, G., Walker, S. I., & Levin, M. (2018). Inform: Efficient information-theoretic
842 analysis of collective behaviors. *Frontiers in Robotics and AI*, 5, 60.

843 Mr, J., Iyer, E. S., Tse, Y.-C., Sorensen, J., Wu, S., Eid, R. S., Cvetkovska, V., Wassef, K., Gostlin,
844 S., Vitaro, P., Spencer, N. J., & Bagot, R. C. (2024). Sex-biased neural encoding of threat
845 discrimination in nucleus accumbens afferents drives suppression of reward behavior. *Nature
846 Neuroscience*, 27(10), 1966–1976. <https://doi.org/10.1038/s41593-024-01748-7>

847 Mr, J., Tse, Y. C., Iyer, E. S., Biris, J., Cvetkovska, V., Lopez, J., & Bagot, R. C. (2020). Ventral
848 Hippocampal Afferents to Nucleus Accumbens Encode Both Latent Vulnerability and Stress-
849 Induced Susceptibility. *Biological Psychiatry*, 88(11), 843–854.
850 <https://doi.org/10.1016/j.biopsych.2020.05.021>

851 Nguyen, A. T., Xu, J., Luu, D. K., Zhao, Q., & Yang, Z. (2019). Advancing System Performance with
852 Redundancy: From Biological to Artificial Designs. *Neural Computation*, 31(3), 555–573.
853 https://doi.org/10.1162/neco_a_01166

854 Y., Daw, N. D., Joel, D., & Dayan, P. (2007). Tonic dopamine: Opportunity costs and the control of
855 response vigor. *Psychopharmacology*, 191(3), 507–520. <https://doi.org/10.1007/s00213-006-0502-4>

85 Bonnell, P., & Grace, A. (1995). Synaptic interactions among excitatory afferents to nucleus
859 accumbens neurons: Hippocampal gating of prefrontal cortical input. *The Journal of*
860 *Neuroscience*, 15(5), 3622–3639. <https://doi.org/10.1523/JNEUROSCI.15-05-03622.1995>

861 Bis, J. M., Namboodiri, V. M. K., Matan, A. M., Voets, E. S., Mohorn, E. P., Kosyk, O., McHenry, J. A.,
862 Robinson, J. E., Resendez, S. L., Rossi, M. A., & Stuber, G. D. (2017). Prefrontal cortex output
863 circuits guide reward seeking through divergent cue encoding. *Nature*, 543(7643), Article 7643.
864 <https://doi.org/10.1038/nature21376>

865 Boker, N. F., Baidya, A., Cox, J., Haetzel, L. M., Zhukovskaya, A., Murugan, M., Engelhard, B.,
866 Goldman, M. S., & Witten, I. B. (2022). Choice-selective sequences dominate in cortical relative
867 to thalamic inputs to NAc to support reinforcement learning. *Cell Reports*, 39(7).
868 <https://doi.org/10.1016/j.celrep.2022.110756>

869 Coli, V., Terrier, J., Espallergues, J., Valjent, E., O'Connor, E. C., & Lüscher, C. (2014). Contrasting
870 forms of cocaine-evoked plasticity control components of relapse. *Nature*, 509(7501), Article
871 7501. <https://doi.org/10.1038/nature13257>

872 Chiatelli, M., Tejeda, H. A., Barker, D. J., Bontempi, L., Wu, J., Lopez, A., Palma Ribeiro, S.,
873 Lucantonio, F., Parise, E. M., Torres-Berrio, A., Alvarez-Bagnarol, Y., Marino, R. A. M., Cai, Z.-
874 L., Xue, M., Morales, M., Tamminga, C. A., Nestler, E. J., & Bonci, A. (2021). Cooperative
875 synaptic and intrinsic plasticity in a disynaptic limbic circuit drive stress-induced anhedonia and
876 passive coping in mice. *Molecular Psychiatry*, 26(6), Article 6. <https://doi.org/10.1038/s41380-020-0686-8>

877 Ed, S. J., Lafferty, C. K., Mendoza, J. A., Yang, A. K., Davidson, T. J., Grosenick, L., Deisseroth, K.,
878 & Britt, J. P. (2018). Coordinated Reductions in Excitatory Input to the Nucleus Accumbens
879 Underlie Food Consumption. *Neuron*, 99(6), 1260-1273.e4.
880 <https://doi.org/10.1016/j.neuron.2018.07.051>

881 Spellman, T., Svei, M., Kaminsky, J., Manzano-Nieves, G., & Liston, C. (2021). Prefrontal deep
882 projection neurons enable cognitive flexibility via persistent feedback monitoring. *Cell*, 184(10),
883 2750-2766.e17. <https://doi.org/10.1016/j.cell.2021.03.047>

884 Shieh, J. H., Kim, H., Huh, N., Lee, D., & Jung, M. W. (2010). Distinct Roles of Rodent Orbitofrontal and
885 Medial Prefrontal Cortex in Decision Making. *Neuron*, 66(3), 449–460.
886 <https://doi.org/10.1016/j.neuron.2010.03.033>

887 Benzel, J. M., Zlebnik, N. E., Patton, M. H., Smethells, J. R., Ayvazian, V. M., Dantrassy, H. M., Zhang, L.-Y.,
888 Mathur, B. N., & Cheer, J. F. (2023). Selective chemogenetic inactivation of
889 corticoaccumbal projections disrupts trait choice impulsivity. *Neuropsychopharmacology*,
890 48(12), Article 12. <https://doi.org/10.1038/s41386-023-01604-5>

891 Williams, E. S., Manning, C. E., Eagle, A. L., Swift-Gallant, A., Duque-Wilckens, N., Chinnusamy, S.,
892 Moeser, A., Jordan, C., Leininger, G., & Robison, A. J. (2020). Androgen-Dependent
893 Excitability of Mouse Ventral Hippocampal Afferents to Nucleus Accumbens Underlies Sex-
894 Specific Susceptibility to Stress. *Biological Psychiatry*, 87(6), 492–501.
895 <https://doi.org/10.1016/j.biopsych.2019.08.006>

896 Shida, K., Drew, M. R., Kono, A., Mimura, M., Takata, N., & Tanaka, K. F. (2021). Chronic social
897 defeat stress impairs goal-directed behavior through dysregulation of ventral hippocampal
898 activity in male mice. *Neuropsychopharmacology*, 46(9), 1606–1616.
899 <https://doi.org/10.1038/s41386-021-00990-y>

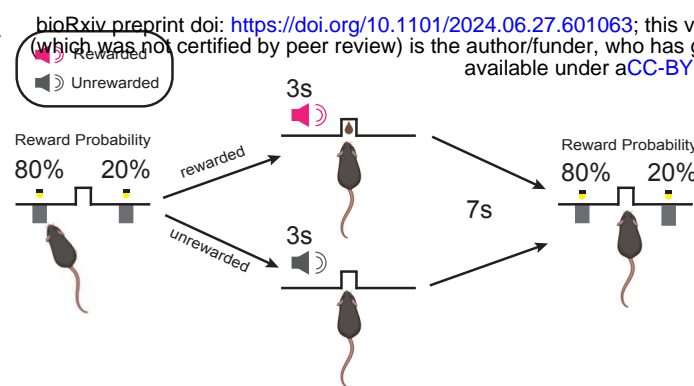
901 Shida, K., Drew, M. R., Mimura, M., & Tanaka, K. F. (2019). Serotonin-mediated inhibition of ventral
902 hippocampus is required for sustained goal-directed behavior. *Nature Neuroscience*, 22(5),
903 Article 5. <https://doi.org/10.1038/s41593-019-0376-5>

904 Shida, K., Tsutsui-Kimura, I., Kono, A., Yamanaka, A., Kobayashi, K., Watanabe, M., Mimura, M., &
905 Tanaka, K. F. (2020). Opposing Ventral Striatal Medium Spiny Neuron Activities Shaped by
906 Striatal Parvalbumin-Expressing Interneurons during Goal-Directed Behaviors. *Cell Reports*,
907 31(13), 107829. <https://doi.org/10.1016/j.celrep.2020.107829>

908 Z., Guindani, M., Grieco, S. F., Chen, L., Holmes, T. C., & Xu, X. (2022). Beyond t test and
909 ANOVA: Applications of mixed-effects models for more rigorous statistical analysis in
910 neuroscience research. *Neuron*, 110(1), 21–35. <https://doi.org/10.1016/j.neuron.2021.10.030>

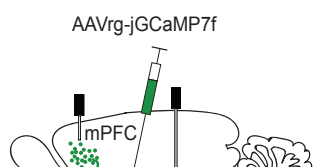
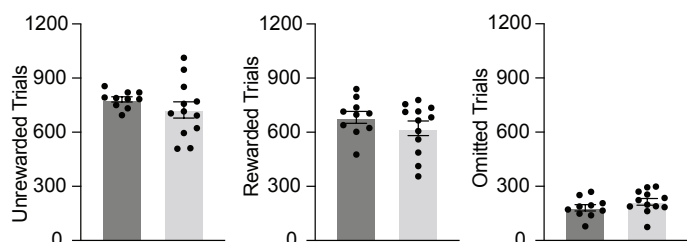
911 Ismaier, A. K., Dong, Y., & Huang, Y. H. (2022). Cocaine-induced projection-specific and cell type-
912 specific adaptations in the nucleus accumbens. *Molecular Psychiatry*, 27(1), Article 1.
913 <https://doi.org/10.1038/s41380-021-01112-2>

914

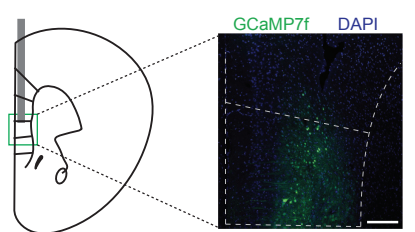


B The copyright holder for this preprint (which was not certified by peer review) is the author/funder, who has granted bioRxiv a license to display the preprint in perpetuity. It is made available under aCC-BY 4.0 International license.

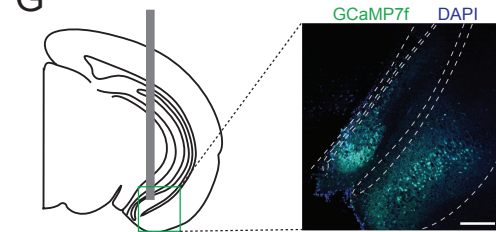
C Female **D** Male



F



G

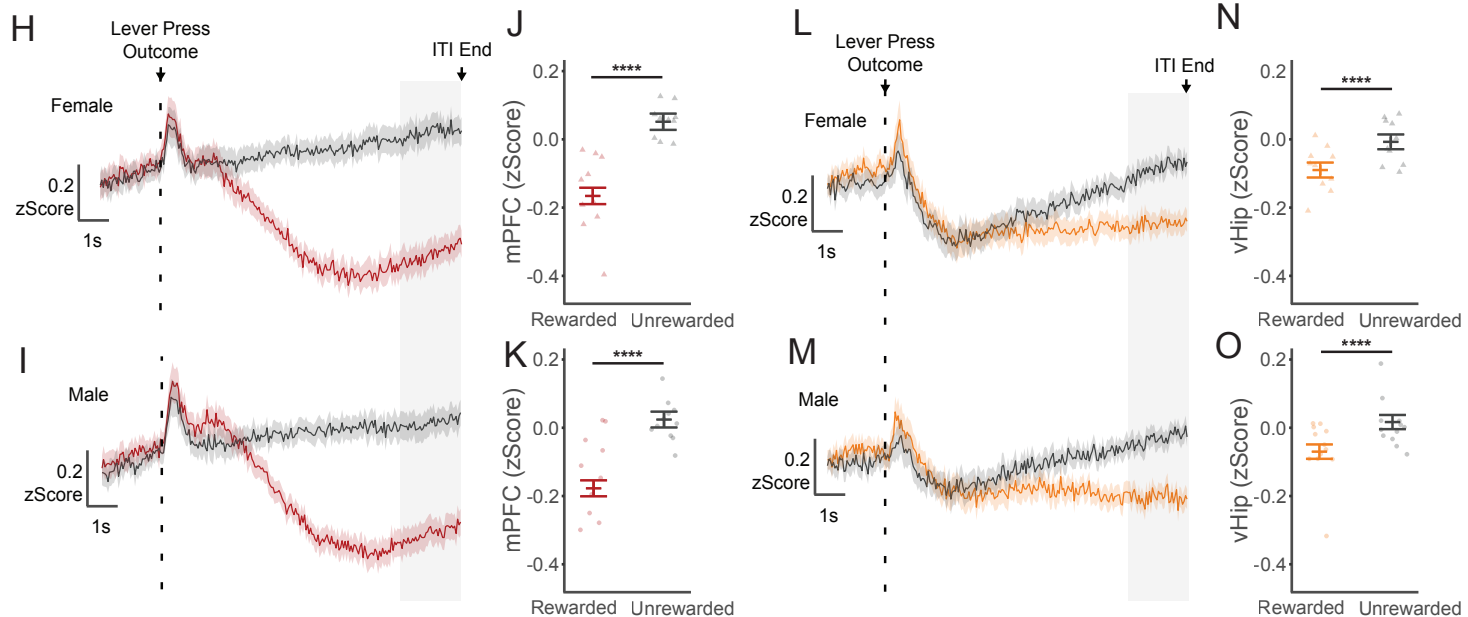


mPFC-NAc

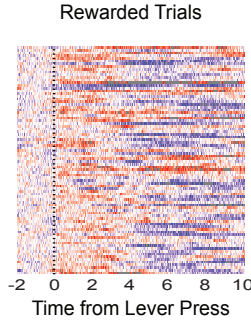
— Red — Unrewarded

vHip-NAc

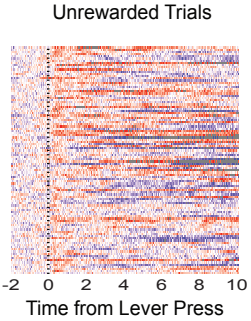
— Orange — Unrewarded



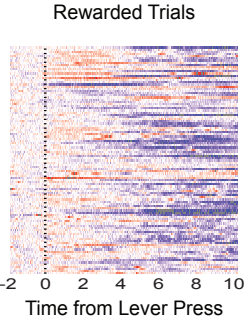
P **R**



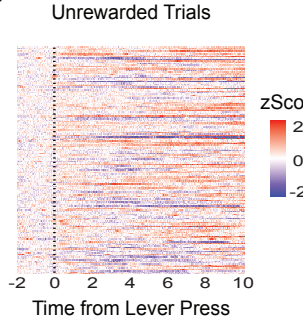
Q



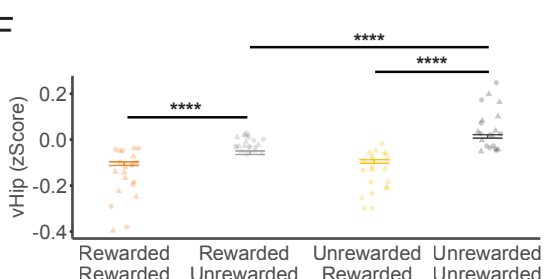
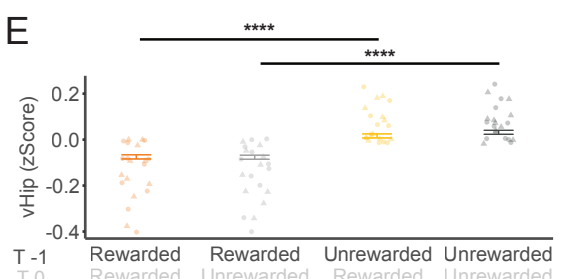
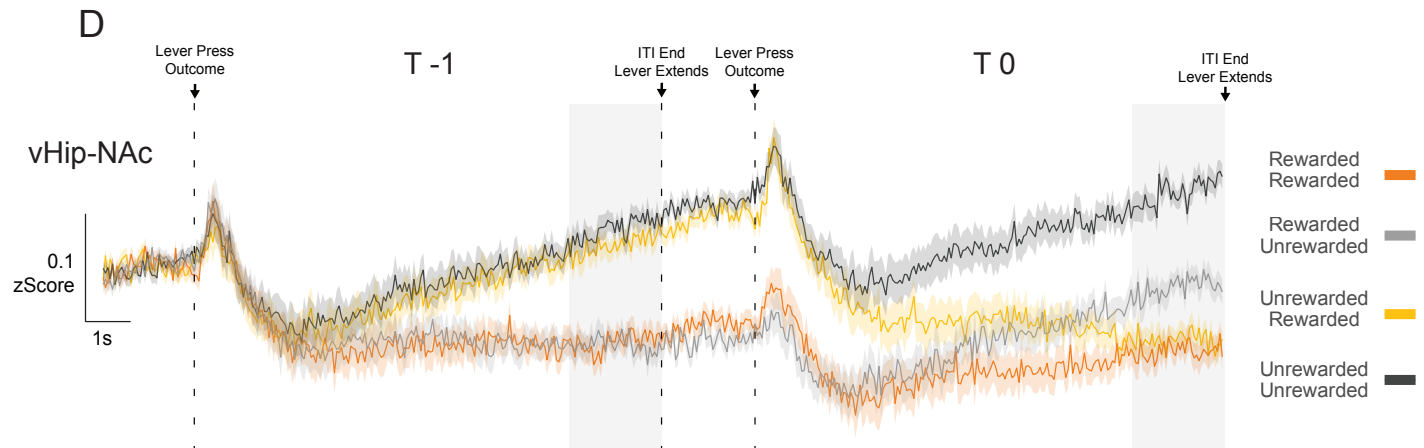
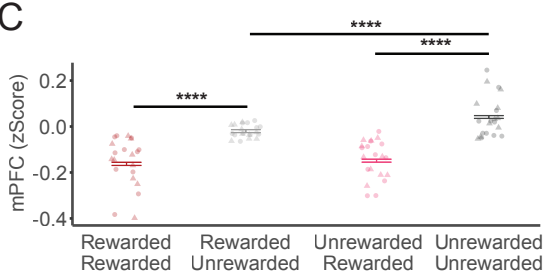
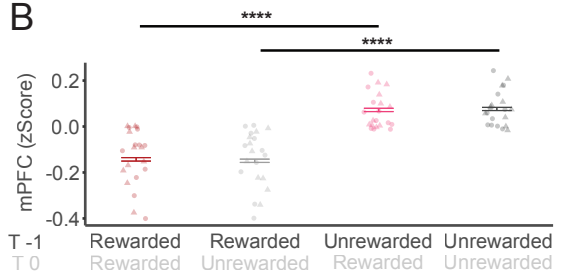
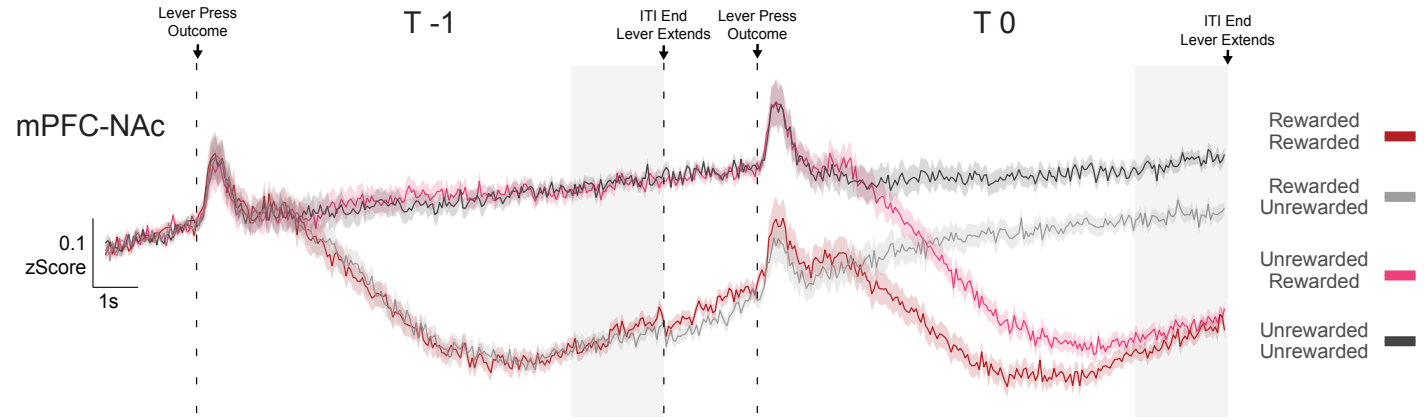
R **S**

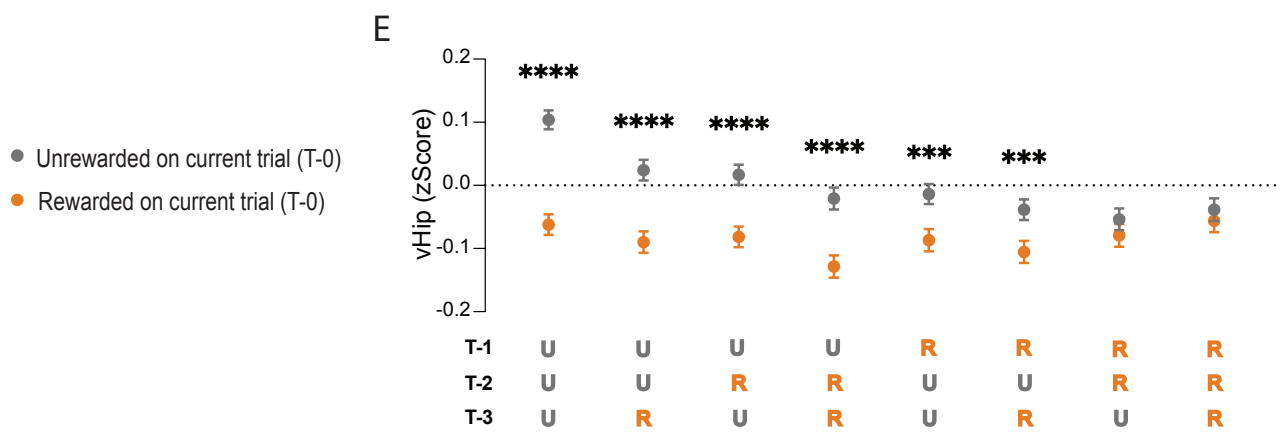
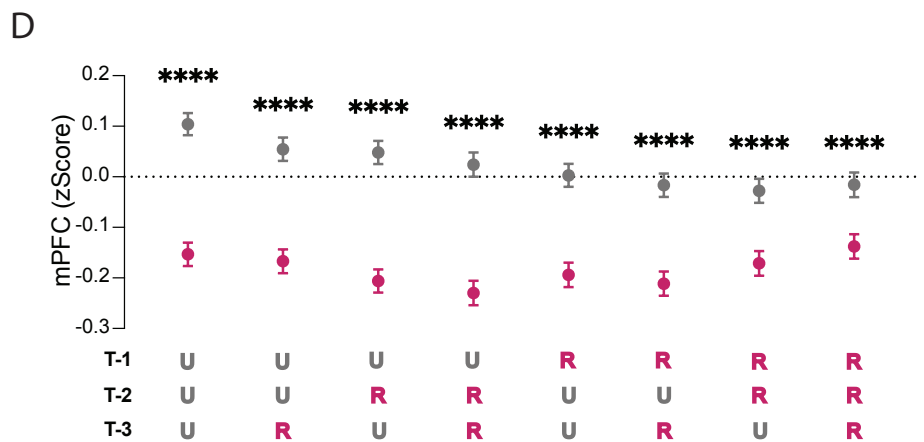
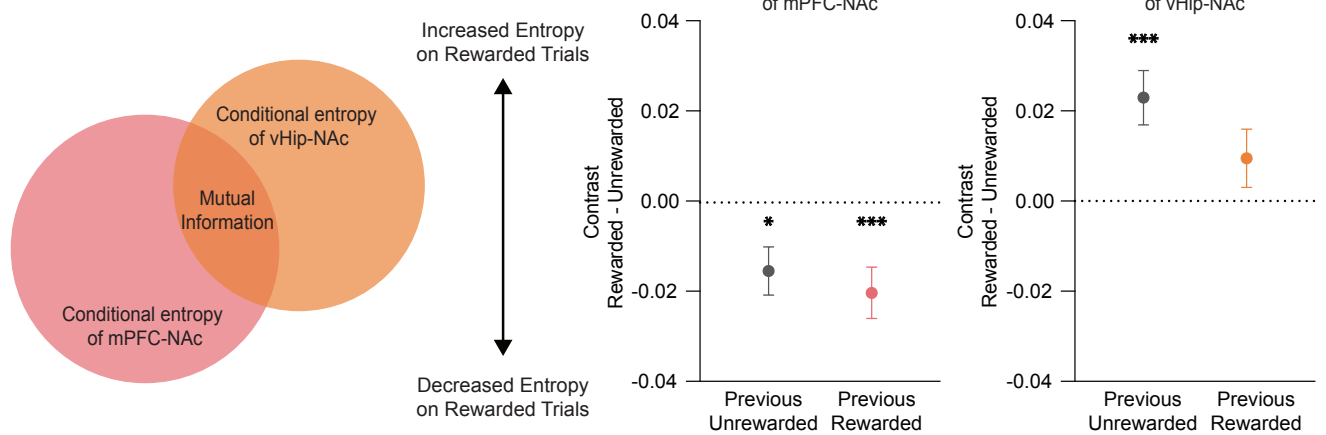


S

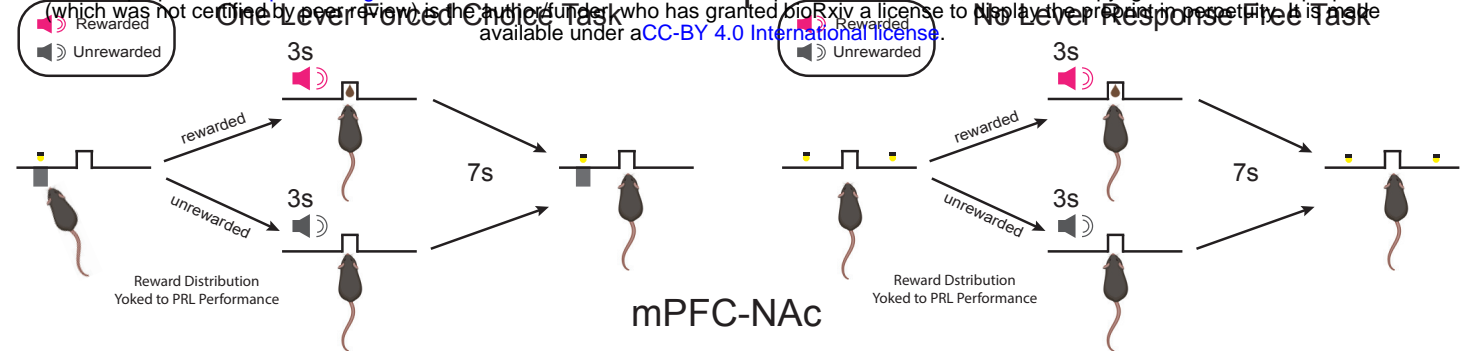


zScore
2
0
-2

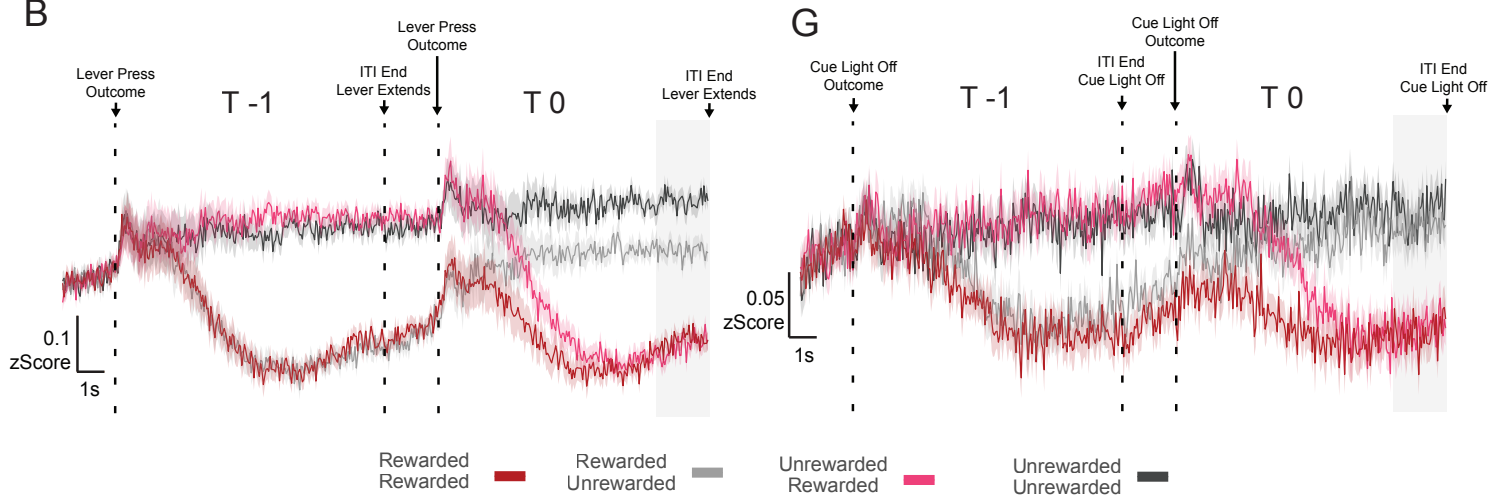




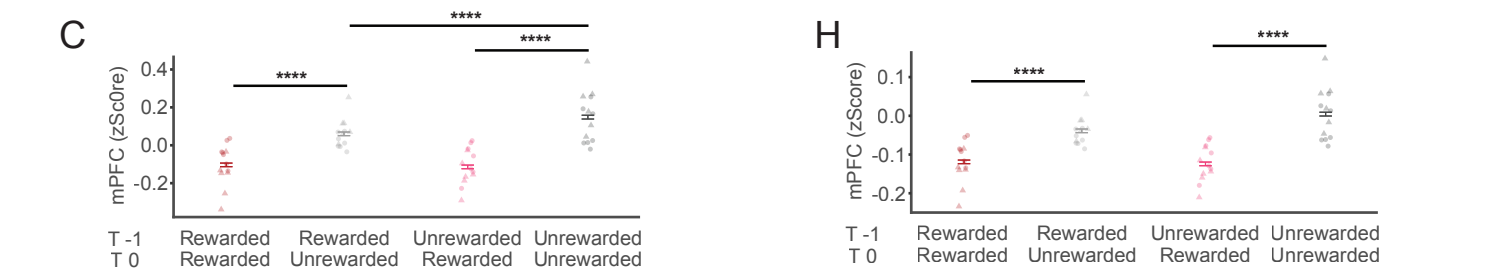
A



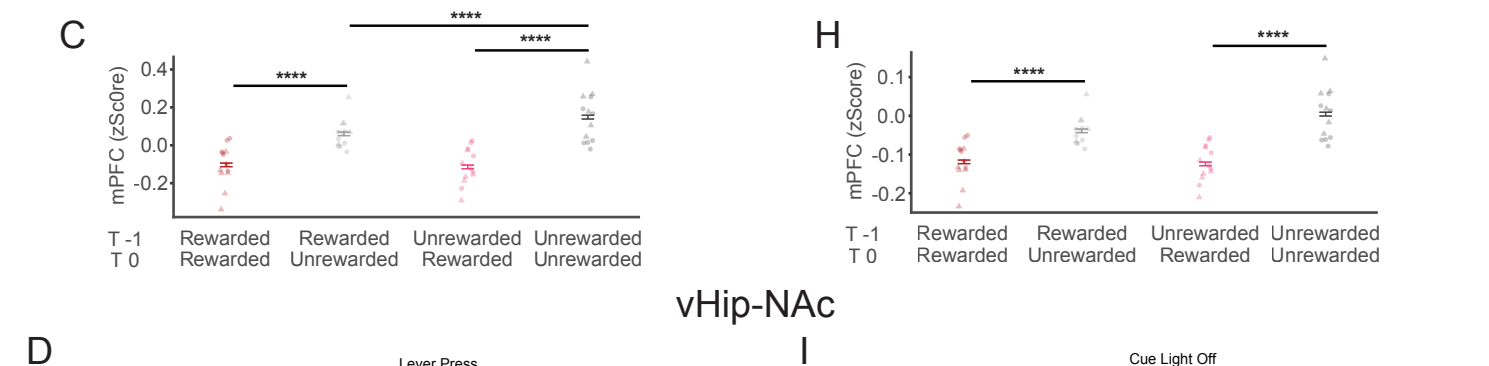
B



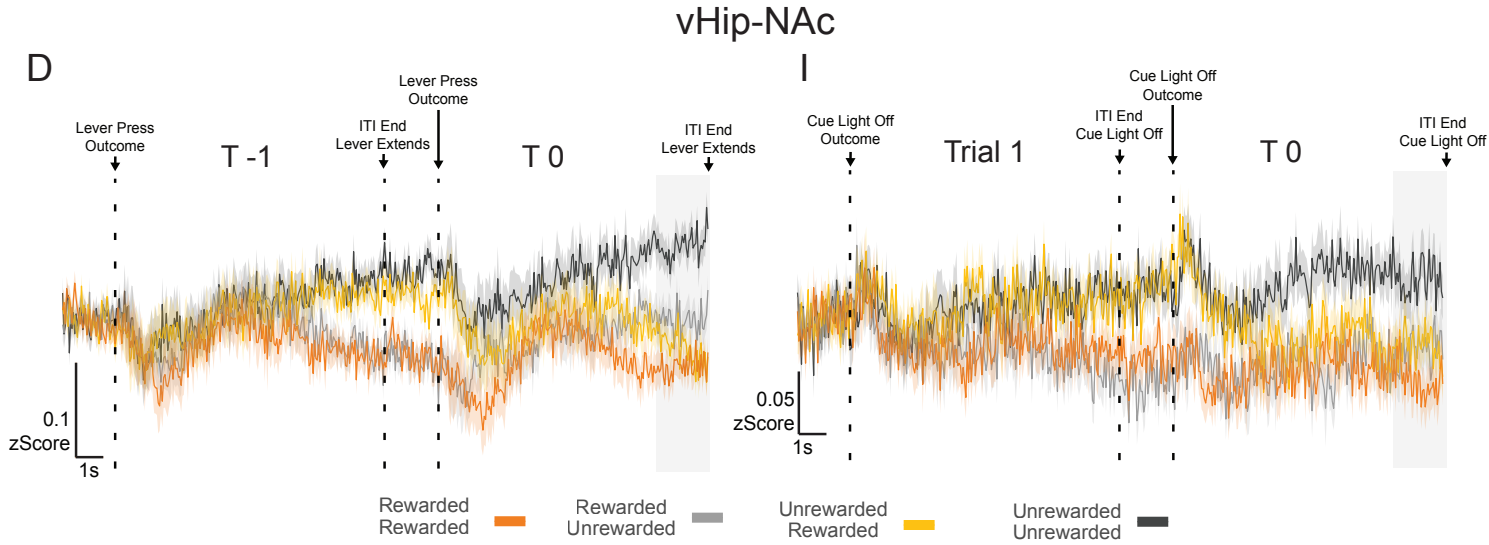
G



H



D



vHip-NAc

E



